Biosensors and Bioelectronics 134 (2019) 49–56

Contents lists available at ScienceDirect

Biosensors and Bioelectronics

journal homepage: www.elsevier.com/locate/bios

Electrochemical dual-aptamer-based biosensor for nonenzymatic detection of cardiac troponin I by nanohybrid electrocatalysts labeling combined with DNA nanotetrahedron structure

Duanping Sun[a,b,c,d,*], Zibin Luo[d], Jing Lu[d,**], Shangshi Zhang[a], Tong Che[a], Zuanguang Chen[d], Luyong Zhang[a,b,c,***]

[a] Center for Drug Research and Development, Guangdong Pharmaceutical University, Guangzhou, 510006, China
[b] Guangzhou Key Laboratory of Construction and Application of New Drug Screening Model Systems, Guangdong Pharmaceutical University, Guangzhou, 510006, China
[c] Key Laboratory of New Drug Discovery and Evaluation of Ordinary Universities of Guangdong Province, Guangdong Pharmaceutical University, Guangzhou, 510006, China
[d] School of Pharmaceutical Sciences, Sun Yat-Sen University, Guangzhou, 510006, China

ARTICLE INFO

Keywords:
Electrochemical aptasensor
Dual aptamer
Cardiac troponin I
Magnetic metal organic framework

ABSTRACT

The accurate detection of biomarkers for acute myocardial infarction (AMI) plays an important role in clinical diagnosis and management process. In this work, we developed an electrochemical biosensor by using magnetic metal organic framework (MMOF) nanocatalysts and DNA nanotetrahedron (NTH) based dual-aptamer probes for nonenzymatic detection of cardiac troponin I (cTnI), a gold standard biomarker for the early diagnosis of AMI. Firstly, the NTH-assisted dual-aptamer (Tro4 and Tro6) capture probes were immobilized on the screen-printed gold electrode (SPGE) for the highly enhanced capture the target cTnI with steady support and optimized interface density. Then, the MMOF Fe_3O_4@UiO-66 nanozymes were decorated by bimetallic Cu@Au nanoparticles and two kinds of aptamer. This fabricated nonenzymatic nanoprobe1 (NP1) can be applied for recognizing the cTnI specifically and amplifying the current signal by catalyzing the oxidation of hydroquinone (HQ) to benzoquinone (BQ) with H_2O_2. The target proteins were captured to fabricate a supersandwich-like structure on a SPGE interface. Furthermore, the nanoprobe2 (NP2) of Cu@Au nanozymes labeled with dual-complementary DNA (cDNA) to the dual-aptamer, were anchored on the NP1 through DNA hybridization, leading to the formation of cluster-based nanoprobes for further enhancing detection sensitivity. Finally, this enzyme-free electrochemical aptasensor exhibited great analytical performance with a dynamic range of 0.05–100 ng/mL, a low detection limit of 16 pg/mL, high selectivity and good repeatability. The fabricated aptasensor has great potential development in the field of clinic disease diagnostics for AMI.

1. Introduction

Cardiovascular disease has turned into a severe public health problem worldwide, especially acute myocardial infarction (AMI) is a leading clinical disease and would cause serious damage in the myocardium (Smith and Gerszten, 2017). Following the myocardial damage, the individual proteins of troponin complex are released into the bloodstream within 90 min to 3 h upon symptom onset of AMI (Nandhikonda and Heagy, 2011). Early diagnosis of AMI play a vital role in clinical research for persons at high cardiovascular risk. Cardiac biomarkers can improve identification of high-risk patients for AMI events. A variety of cardiac biomarkers, including creatine kinase-MB (CK-MB), cardiac troponin T (cTnT), cardiac troponin I (cTnI) and myoglobin (MYO), can be employed to diagnose an AMI (Abdorahim et al., 2016; Nezami et al., 2018; Rezaei et al., 2016). Among various biomarkers, cTnI is regarded as the “gold standard” marker for AMI (Kemp et al., 2004; Takeda et al., 2003). Patients with a clear positive test for AMI have serum levels of cTnI as high as 5–50 ng/mL. Therefore, numerous studies have been performed to obtain reliable and sensitivity diagnostic tools for cTnI detection (Han et al., 2016).

Various developed methods, such as electrochemistry immunoassay (Akter et al., 2017; Dhawan et al., 2018; Yan et al., 2018; Zhang et al.,

* Corresponding author. Center for Drug Research and Development, Guangdong Pharmaceutical University, Guangzhou, 510006, China.
** Corresponding author.
*** Corresponding author. Center for Drug Research and Development, Guangdong Pharmaceutical University, Guangzhou, 510006, China.
E-mail addresses: sundp@gdpu.edu.cn (D. Sun), lujing0504@126.com (J. Lu), lyzhang@gdpu.edu.cn (L. Zhang).

https://doi.org/10.1016/j.bios.2019.03.049
Received 23 February 2019; Received in revised form 21 March 2019; Accepted 23 March 2019
Available online 29 March 2019
0956-5663/

2018a), photoelectrochemical immunoassay (Fan et al., 2018; Tan et al., 2017), electrochemiluminescence immunoassay (Yang et al., 2018b; Zhang et al., 2017), fluorescence immunoassay (Liu et al., 2018a) and enzyme-linked immunosorbent assay (ELISA), were utilized for the determination of cTnI. Compared with other approaches, electrochemical immunoassay has attracted particular attention due to its properties of portable, sensitive, and rapid response. However, these antibody based methods have several limitations such as the difficulty for the chemical modification, high cost for the production, and low stability at high temperatures. Recently, electrochemical aptamer-based biosensor has been established for cTnI research as they offer many advantages to overcome the limitations of antibodies (Chekin et al., 2018; Negahdary et al., 2017; Qiao et al., 2018). Aptamers are single-stranded RNA or DNA oligonucleotides that can specifically and efficiently bind to a series of proteins and cells. For instance, Ban's group has demonstrated that Tro4 and Tro6 aptamer can be used for recognizing cTnI selectively (Jo et al., 2015, 2017). Compared with antibodies, aptamers have been widely performed in the biosensor fields with high affinity, good stability, small size, and flexible modification. Hence, dual-aptamer as recognition molecule on the electrode interface can increase the recognition efficiency and target accessibility for cTnI analysis.

However, single-stranded DNA aptamer is easy to nonspecifically absorb and aggregate on the electrode interface, impeding the effective binding of aptamers to target proteins. Framework nucleic acids especially DNA nanotetrahedron (NTH) structure with well-defined and highly rigid architectures can ensure the precise orientation and density of the aptamer on the sensing interface (Goodman et al., 2005). DNA NTH structure is assembled from four single-stranded nucleic acids and can be firmly attached on the electrode surface uniformly. The relative far vertical space between aptamer and electrode can provide a solution-native-like recognition microenvironment and suppress the entangling of aptamer recognition probes. Because of the superior properties of NTH-based electrode surface, it has been used for sensitive and selective detection of protein, exosome and cell (Lin et al., 2016; Sun et al., 2018a, 2018b; Yang et al., 2018a). Herein, NTH-based dual-aptamer capture probe on the electrode surface can greatly increase the target protein accessibility and recognition efficiency, and further improve detection sensitivity of aptasensor for cTnI detection.

Only with the DNA NTH structure, the detection sensitivity for cTnI may not meet the requirement of clinical sample assay. For electrochemical aptasensing, the detection sensitivity can be improved with specifically designed nanoprobes. The common signal amplification method is to immobilize natural enzymes onto nanomaterials for enhancing the detection sensitivity through enzymatic electrochemical processes (Sun et al., 2016; Zheng et al., 2014). However, the native conformations of enzymes can be easily disrupted by changes of pH and temperature, leading to the loss of catalytic activities. In addition, the preparation and storage of nature enzymes are expensive and time-consuming. Hence, it is urgently desirable to design robust nonenzymatic nanocatalysts with high electrocatalytic activities for electrochemical biosensor.

Recently, nanozymes, a term defined for nanomaterial with enzyme-mimicking properties, have emerged as a new kind of artificial enzymes due to its striking merits of low cost, robustness and ease of mass production (Liu et al., 2018b; Wei and Wang, 2013). In 2007, it was discovered that magnetic iron oxide (Fe_3O_4) nanoparticles possess an intrinsic enzyme-like activity similar to that of natural horseradish peroxidase (HRP) (Zheng et al., 2014). To date, a large amount of nanomaterials have been demonstrated to possess the HRP-mimicking properties, ranging from metals and metal oxides to metal organic frameworks (MOFs) (Wang et al., 2018; Zhang et al., 2018b). For instance, noble metal-related nanomaterials (Au, Pt and Pd) have extensive applications owing to the great catalytic ability and high ratio surface area. Especially, core-shell bimetallic nanoparticles have showed outstanding catalytic property over the corresponding monometallic nanomaterials (Sun et al., 2016). In addition, MOFs, an emerging class of porous crystalline material, have received increasing attention owing to unique properties of permanent porosity, tunable pore sizes and high interface area. Furthermore, MOFs coupled with other nanomaterials has become a hot pursuit (Song et al., 2017; Zhao et al., 2016). This is because the novel hybrid nanomaterials readily inherit the advantages of both parent materials, significantly boosting their applications. Therefore, by the combination of magnetic metal organic framework (MMOF) nanocomposites and core-shell bimetallic nanoparticles, the nanohybrid electrocatalysts can be performed as the nanocarriers to immobilize aptamer for amplifying electrochemical signals. Compared with Fe_3O_4 magnetic nanoparticles, the nanoelectrocatalysts exhibited outstanding catalytic performance since the MOFs and bimetallic nanoparticles can greatly improve the catalytic activity of Fe_3O_4 nanoparticles (Ma et al., 2018).

In this work, an enzyme-free electrochemical biosensor was proposed for cTnI detection based on NTH-based dual-aptamer as capture probe and hybrid nanoelectrocatalysts as signal amplification probe. Firstly, the self-assembled NTH-based Tro4 and Tro6 aptamer probes were conjugated on a screen-printed gold electrode (SPGE) interface through gold − thiol interactions for the greatly enhanced recognition of cTnI. Then, the nonenzymatic nanoprobe1 (NP1) was fabricated through the two kinds of aptamer immobilized on the surfaces of bimetallic Cu@Au nanoparticles modified MMOF Fe_3O_4@UiO-66 (Fe_3O_4@UiO-66/Cu@Au). The target cTnI were captured to fabricate an NTH-dual-aptamer/cTnI/NP1 supersandwich-like structure on a SPGE interface. Furthermore, the nanoprobe2 (NP2) of Cu@Au nanoparticles labeled with two types of complementary DNA (cDNA) to the dual-aptamer, were immobilized on the NP1 via the DNA hybridization, leading to the formation of cluster-based nanoprobes. The cluster-based nanoprobes can be applied to catalyze the oxidation of hydroquinone (HQ) for amplifying the electrochemical signal and improving the detection sensitivity significantly. As a result, the aptasensor exhibited outstanding sensitivity and selectivity for cTnI, showing great potential applications in the clinic diagnosis.

2. Experimental section

2.1. Materials and apparatus

All oligonucleotides were synthesized and purified by Invitrogen Biotech. Co., Ltd. (Shanghai China). The sequences were showed in Table S1. Recombinant cardiac troponin I (cTnI), recombinant myoglobin (MYO), bovine serum albumin (BSA) and ELISA kit for cTnI were purchased from Cloud-clone Co., Ltd. (Wuhan, China). Other detailed chemicals and apparatus are provided in the Supplementary material.

2.2. Synthesis of hybrid nanoprobes

According to the reported methods, Fe_3O_4@UiO-66/Cu@Au nanomaterials were prepared. Detailed steps are provided in the Supplemental material. Firstly, the synthesized Fe_3O_4@UiO-66/Cu@Au nanocomposites (1 mg) were dispersed in 1 mL phosphate buffered saline (PBS) solution. Then, 25 μL Tro4 aptamer (5 μM) and 25 μL Tro6 aptamer (5 μM) were added to the solution and reacted for 24 h at 4 °C under stirring. Subsequently, BSA (1%, w/v) was added to block the interface of the nanoparticles and the product was washed with PBS buffer for several times. Lastly, the synthesized Fe_3O_4@UiO-66/Cu@Au-Tro4-Tro6-BSA hybrid NP1 were stored in PBS solution (pH 7.4, 10 mM) at 4 °C for further use. Based on the same condition, the synthesized Cu@Au-cDNA1-cDNA2-BSA hybrid NP2 were fabricated and stored in PBS solution (pH 7.4, 10 mM) at 4 °C.

2.3. Construction of the NTH-based aptasensing interface

Before the assembly of NTH, the monomers (a, b, c, d1-Tro4 and d2-

Tro6) were treated with 10 mM TCEP for 2 h to cleave the disulfide linkage. Then the DNAs were mixed equivalently in TM buffer, heated at 95 °C for 10 min, and rapidly cooled at 4 °C for 10 min. The formation of two types of NTHs including NTH-Tro4 and NTH-Tro6 were analyzed with agarose gel electrophoresis.

In order to construct the aptasensing interface, 10 μL of 1.25 μM NTH-based dual-aptamer probe, which was prepared by mixing NTH-Tro4 and NTH-Tro6 in equal proportions, was dropped on the interface of SPGE and incubated at 4 °C overnight. The electrode was washed with ultrapure water gently to remove the unbound NTH. Then 10 μL of 1 mM 6-mercapto-1-hexanol (MCH) was added onto the SPGE interface to block the blank sites at room temperature for 2 h.

2.4. Electrochemical measurement

After being rinsed with ultrapure water, the modified electrode was incubated with 100 μL of cTnI with different concentrations for 60 min at 37 °C to recognize cTnI specifically. The cTnI-captured electrode was rinsed with PBS solution carefully to remove the dissociative cTnI. Afterward, 10 μL of NP1 was dropped and incubated for 60 min at 37 °C to form supersandwich-type aptasensor. Then the electrode was washed with PBS solution lightly for removing nonspecifically bound NP1. 10 μL of NP2 was dropped on the SPGE surface and incubated for 30 min at 37 °C to form the cluster-based nanoprobes via the hybridization of aptamer and cDNA. The differential pulse voltammetry (DPV) measurements was performed in degassed PBS (pH 7.0, 100 mM) containing 3 mM HQ and 2 mM H_2O_2 with potential ranging from 0.1 to −0.3 V and a pulse amplitude of 50 mV.

3. Results and discussion

3.1. Principle of the electrochemical aptasensor

The design principle of the nonenzymatic electrochemical aptasensor is exhibited in Scheme 1. In this paper, a designed nanohybrid electrocatalyst were fabricated through a layer-by-layer (LBL) assembly process. UiO-66, one class of Zr(IV)-based MOFs, is constructed with zirconium ions and terephthalic acid and has attracted great attention due to the chemical and solvent stability. Furthermore, UiO-66 was selected for fabricating the shell over the Fe_3O_4 nanoparticles to form novel MMOF Fe_3O_4@UiO-66. In addition, a kind of bimetallic copper-gold (Cu@Au) nanoparticle was also synthesized. Both MMOF Fe_3O_4@UiO-66 nanocomposites and bimetallic Cu@Au nanoparticles exhibit the HRP-like activities toward the small dye molecules with high specific surface area (Ye et al., 2015; Zhao et al., 2016). The hybrid Fe_3O_4@UiO-66/Cu@Au nanomaterials exhibited outstanding catalytic performance since the UiO-66 and Cu@Au nanoparticles can greatly improve the catalytic activity of Fe_3O_4 nanoparticle. And the hybrid nanomaterials were employed as nanocarriers to load two kinds of aptamer. As a result, the designed nanoprobes are capable of amplifying the electrochemical signal and capturing the target cTnI.

As shown in Scheme 1, the NTH-based dual-aptamer probe was conjugated on the SPGE interface for highly enhanced capture the target cTnI with steady support and optimized interface density. After the target cTnI were captured, the Fe_3O_4@UiO-66/Cu@Au-Tro4-Tro6-BSA hybrid NP1 were assembled to form the supersandwich-like architecture. Furthermore, the Cu@Au-cDNA1-cDNA2-BSA hybrid NP2 were immobilized on the NP1 through DNA hybridization of aptamer and cDNA, leading to the formation of cluster-based nanoprobes to further enhanced signal response. The signal amplification strategy of the nonenzymatic electrochemical aptasensor was depended on the electrochemical reduction of benzoquinone (BQ) from the oxidation of HQ with H_2O_2, which was catalyzed by numerous HRP-mimicking Fe_3O_4@UiO-66 and Cu@Au nanozymes of the cluster-based nanoprobes. The peak current was related to the amount of nanoprobes on the electrode surface. The process is shown as below

$$H_2O_2 + H_2Q \rightarrow Q + 2H_2O$$

$$Q + 2H^+ + 2e^- \rightarrow H_2Q$$

where H_2Q is hydroquinone and Q is benzoquinone.

3.2. Characterization of the nanomaterials

The nanohybrid electrocatalysts were prepared through a LBL assembly process, as schematically illustrated in Fig. 1A. Based on the amino groups and electrostatic attraction, the surface of the Fe_3O_4@UiO-66 nanocomposites can be decorated with Cu@Au nanoparticles. Firstly, Fe_3O_4 magnetic nanoparticles were synthesized with a hydrothermal method. The transmission electron microscopy (TEM) and scanning electron microscope (SEM) images of Fe_3O_4 nanoparticles were shown in Fig. 1B and C. The as-synthesized Fe_3O_4 nanoparticles

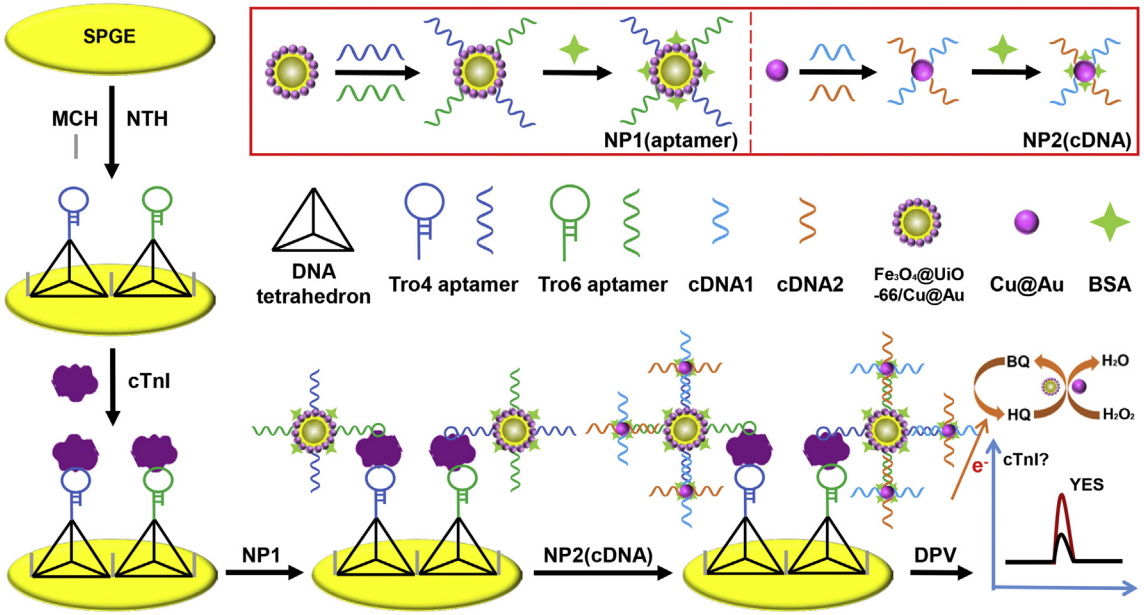

Scheme 1. Schematic illustration of the assembly process of the nonenzymatic nanoprobes and the electrochemical aptasensor for the capture and detection of cTnI.

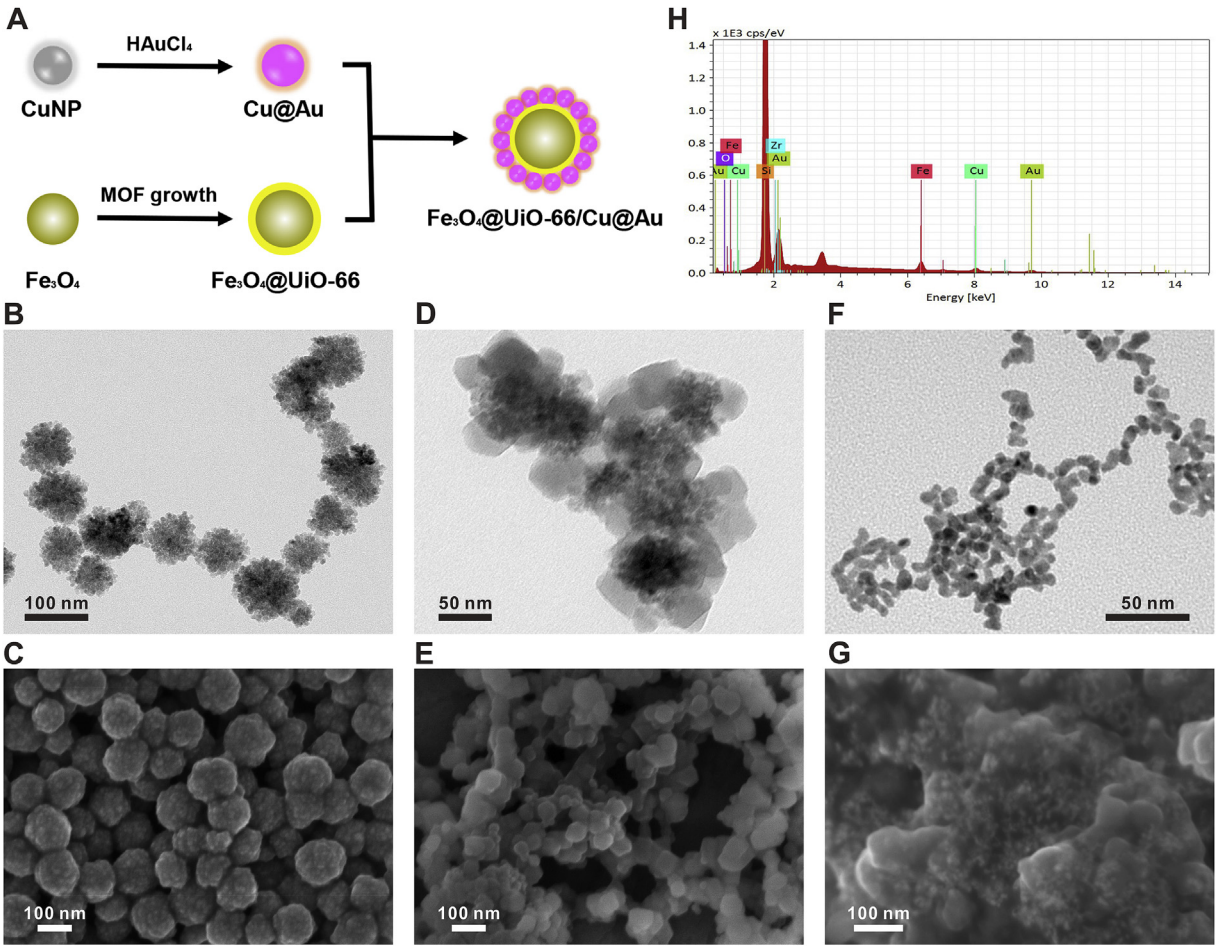

Fig. 1. (A) Schematic illustration of the fabrication of Fe_3O_4@UiO-66/Cu@Au hybrid nanomaterials. SEM images of (B) Fe_3O_4 nanoparticles, (D) Fe_3O_4@UiO-66 nanocomposites and (F) Cu@Au nanoparticles. TEM images of (C) Fe_3O_4 nanoparticles, (E) Fe_3O_4@UiO-66 nanocomposites and (G) Fe_3O_4@UiO-66/Cu@Au nanocomposites. (H) EDS line image of Fe_3O_4@UiO-66/Cu@Au nanocomposites.

were spherical with a diameter about 90 nm. Then the Fe_3O_4@UiO-66 nanocomposites were synthesized by an in situ self-assembly of UiO-66 on the surface of Fe_3O_4 nanoparticles to obtain the core-shell agent. TEM and SEM analysis in Fig. S1 show that the as-prepared UiO-66 nanomaterials are nanocrystals with sharp hexagonal facets.

The morphology and structure of Fe_3O_4@UiO-66 nanocomposites were examined using TEM, SEM, energy dispersive spectroscopy (EDS), Fourier transform infra-red (FT-IR) and X-ray diffraction (XRD), respectively. As can be seen from the TEM image of Fe_3O_4@UiO-66 (Fig. 1D), an obvious difference between the core and shell was observed wherein the Fe_3O_4 core appeared dark, whereas the UiO-66 shell appeared bright. Compared with the SEM images between Fe_3O_4 nanoparticles and Fe_3O_4@UiO-66 nanocomposites, the morphology of Fe_3O_4 nanoparticles become irregular and angular after being covered with UiO-66 shell (Fig. 1E). Moreover, the elemental mapping analysis and EDS line reveal that the Zr and Fe elements were distributed in the shell and core, respectively (Figs. S2A and B).

The FT-IR spectra of Fe_3O_4 and Fe_3O_4@UiO-66 are presented in Fig. S2C. The results shows that the characteristic peaks of UiO-66 at 1564 cm^{-1}, 1430 cm^{-1}, and 1386 cm^{-1} and Fe_3O_4 at 1633 cm^{-1} and 565 cm^{-1} in the FT-IR spectrum of Fe_3O_4@UiO-66. The peak at 3378 cm^{-1} in the spectrum of Fe_3O_4@UiO-66 belonged to the symmetric stretching absorptions of the primary amine groups in the NH_2–H_2BDC ligands, which further verified the successful growth of the UiO-66 shell on the Fe_3O_4 core. These results indicated the successful formation of the Fe_3O_4@UiO-66 composites. The compositions and crystallinities of the synthesized nanomaterials were investigated using XRD. As exhibited in Fig. S2D, the simultaneous existence of the characteristic peaks of Fe_3O_4 and UiO-66 in the XRD pattern of Fe_3O_4@UiO-66 indicated the successful formation of a UiO-66 shell on the interface of Fe_3O_4 nanoparticles without altering their crystallinity. All the results demonstrated the UiO-66 shell was successfully grew on the interface of the Fe_3O_4 nanoparticles.

The synthesis and morphology of Fe_3O_4@UiO-66/Cu@Au nanocomposites were confirmed by SEM and EDS. Cu@Au nanoparticles were prepared through the reduction of $CuSO_4$ and $HAuCl_4$ in the presence of $NaBH_4$ and sodium citrate. Fig. 1F shows the TEM image of the Cu@Au nanoparticles and the results revealed that the as-prepared nanoparticles were nonspherical and interconnected in shape with an average size of 10 nm. The SEM image of Fe_3O_4@UiO-66/Cu@Au nanoparticles were shown in Fig. 1G. As we can see, a large amount of Cu@Au were successfully connected on the interface of Fe_3O_4@UiO-66. At the same time, the EDS line scanning data and elemental mapping analysis reveal that the elements of Fe, O, Zr, Cu and Au were indispensable for the hybrid nanomaterials (Fig. 1H and Fig. S3). Meanwhile, the adsorption of positively charged UiO-66 on colloidal Fe_3O_4 beads switched the ζ potential to a positive value. Cu@Au nanoparticles with negatively charged interfaces were subsequently attached electrostatically to the interface of the Fe_3O_4@UiO-66 nanocomposites (Fig. S4). Therefore, there results demonstrated that the nanohybrid Fe_3O_4@UiO-66/Cu@Au electrocatalysts had been successfully synthesized.

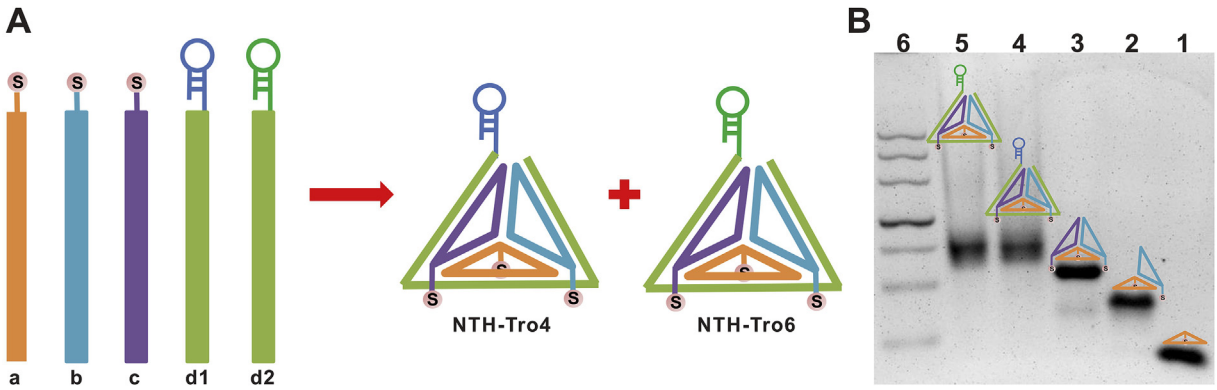

Fig. 2. (A) Schematic illustration of the aptamer-containing NTH structures from four single-stranded DNA sequences. (B) Agarose gel electrophoretic analysis of the gradual formation of NTHs. Lane 1: a; Lane 2: a + b; Lane 3: a + b + c; Lane 4: a + b + c + d1 (NTH-Tro4); Lane 5: a + b + c + d2 (NTH-Tro6); Lane 6: DNA marker.

3.3. Characterization of the NTH-based aptamer probe

The Tro4 and Tro6 aptamer (Fig. S5) were selected for capturing the target cTnI (Jo et al., 2015). As shown in Fig. 2A, DNA NTH structures, self-assembled from four single-stranded nucleic acids, were performed to enhance capture efficiency and detection performance. With the vertex containing exposed aptamer probe and thiol groups at three vertices, the NTH can be firmly attached on the SPGE surface uniformly. Briefly, Tro4 and Tro6 aptamers are built into one of the NTH sequences (d1-Tro4 and d2-Tro6), and the other three (a, b and c) end with thiol groups were conjugated to the electrode through gold – thiol interactions.

The agarose gel electrophoretic result was shown in Fig. 2B to demonstrate the DNA NTH structure. The NTH-Tro4 (lane 4) and NTH-Tro6 (lane 5) migrated more slowly than combinations constructed of fewer than four single-stranded sequences (lane 1, lane 2 and lane 3). As the rapid and specific DNA hybridization ensuring the high yield of NTHs, the only major clear band can be observed on the gel. Therefore, the results demonstrated that our NTH-based aptamer probes have been successfully formed and can be further performed in the following experiments.

3.4. Electrochemical characterization of the proposed aptasensor

DPV characterization was utilized to demonstrate the signal amplification strategy of the electrochemical aptasensor. Fig. S6A shows the DPV curves of the aptasensor in the absence and presence of HQ or H_2O_2. No obvious electrochemical signal can be observed for the NP1/cTnI/MCH/NTH-Tro4 + Tro6/SPGE in a PBS solution (curve a). However, a small peak can be observed related to the reduction of BQ in a PBS solution containing only 3 mM HQ (curve b). When the modified electrode was immersed in the PBS solution containing 3 mM HQ and 2 mM H_2O_2, the peak current increased sharply (curve c), indicating that hybrid nanoprobes in a supersandwich structure exhibits its outstanding HRP-mimicking catalytic activity.

Furthermore, both Tro4 and Tro6 aptamers can be utilized recognition probe for cTnI. Different ratios of the TNH-based Tro4 and Tro6 aptamers were evaluated for cTnI detection. As shown in Fig. 3A, DPV peak current can be observed for the Fe_3O_4@UiO-66/Cu@Au-Tro6-BSA/cTnI/MCH/NTH-Tro6/SPGE (curve a) and Fe_3O_4@UiO-66/Cu@Au-Tro4-BSA/cTnI/MCH/NTH-Tro4/SPGE (curve b) in the detection solution containing 3 mM HQ and 2 mM H_2O_2. However, a more obvious electrochemical peak current can be observed with the NTH-based dual-aptamer capture probes and dual-aptamer modified signal nanoprobes (NP1, curve c). It can be ascribed to combination of Tro4 and Tro6 aptamer can largely improve the capture efficiency and the detection sensitivity.

In addition, as exhibited in Fig. 3B, DPV peak current can be observed for the NP1/cTnI/MCH/NTH-Tro4 + Tro6/SPGE (curve a) in the detection solution. However, larger increase of DPV peak current was observed through the formation of the cluster-based nanoprobes with the cDNA-based NP2 (curve b). Due to the DNA hybridization and LBL assembly method, a large amount of HRP-mimicking nanomaterials can be attached onto the cluster-based nanoprobes for amplifying the signals significantly. Meanwhile, electrochemical impedance spectroscopy (EIS) were performed to understand the electrochemical characterization of this aptasensor. A detailed description can be found in the Supplementary material and Fig. S6B.

3.5. Performance of the proposed aptasensor

The selectivity and sensitivity is an important criterion in the early clinical diagnosis. To evaluate the specificity of the developed aptasensor, different proteins including BSA, MPT64, MYO, and cTnI were tested in this work. The corresponding results are given in Fig. 4A and B. Compared with the blank control, no obvious electrochemical signal can be observed for the separate additions of proteins with the same concentration except for cTnI. These results indicated the selectivity of the aptasensor was acceptable for the detection of cTnI.

As shown in Fig. S7, the regression equation of ELISA method for cTnI is $A = 0.3105 + 0.0019C_{cTnI}$ (pg/mL), with a linear range of 31.2–1000 pg/mL and correlation coefficient of $R^2 = 0.998$. The detection limit is calculated as 10 pg/mL. The proposed aptasensor with different concentrations of cTnI was carried out under the optimal conditions (detailed description in the Supplementary material and Fig. S8). As the concentrations of cTnI increased, the peak current increased gradually. The increasing amount of the cTnI can result in the corresponding increase of binding of nanoprobes onto the electrode surface. Fig. 4C showed the typical DPV current responses with increasing cTnI concentrations from 0.05 ng/mL to 100 ng/mL. There is a good linear correlation between the logarithm values of cTnI concentration (C_{cTnI}) and the DPV current value. As depicted in Fig. 4D, the linear equation is $I\ (\mu A) = 4.483 + 0.936 \lg C_{cTnI}$ (ng/mL) ($R^2 = 0.991$) with a linear range of 0.05–100 ng/mL. And the detection limit is calculated to be 16 pg/mL for cTnI based on the 3σ method.

This detection limit of nonenzymatic electrochemical aptasensor exhibited lower than those of other previous reported methods based on electrochemical aptasensor and ELISA (Table 1). The reasons why the aptasensor has the excellent analytical performance are as follows: Firstly, the NTH-assisted dual-aptamer probes were immobilized on the SPGE for highly enhanced capture the target cTnI. Then the nanohybrid Fe_3O_4@UiO-66/Cu@Au electrocatalysts with multiple HRP-mimic activities were introduced to be nanocarriers for amplifying the signal significantly. Lastly, with the assistance of cDNA-based NP2 and DNA

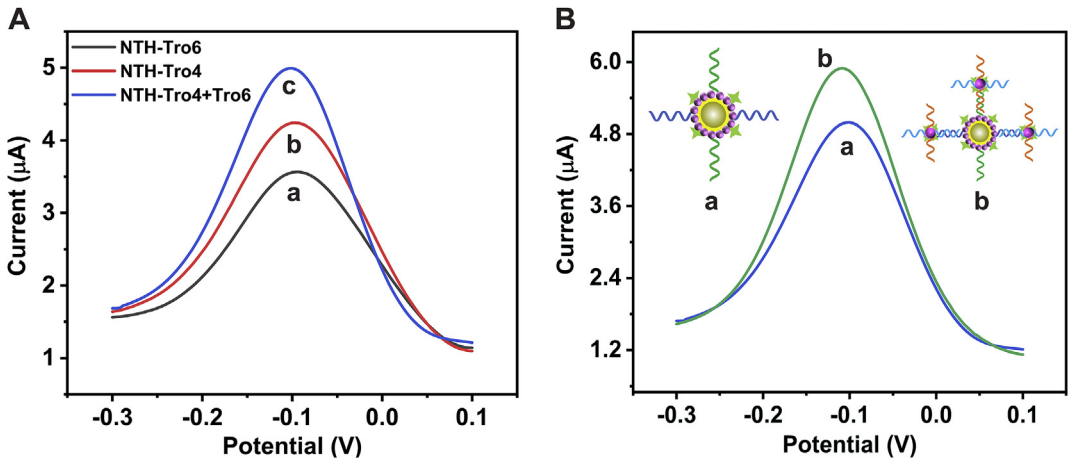

Fig. 3. (A) DPV responses of the (a) Fe_3O_4@UiO-66/Cu@Au-Tro6-BSA/cTnI/MCH/NTH-Tro6/SPGE, (b) Fe_3O_4@UiO-66/Cu@Au-Tro4-BSA/cTnI/MCH/NTH-Tro4/SPGE, and (c) NP1/cTnI/MCH/NTH-Tro4 + Tro6/SPGE in the PBS solution (100 mM, pH 7.0) with 3 mM HQ and 2 mM H_2O_2. (B) DPV responses of the (a) NP1/cTnI/MCH/NTH-Tro4 + Tro6/SPGE and (b) NP1 + NP2/cTnI/MCH/NTH-Tro4 + Tro6/SPGE in the PBS solution (100 mM, pH 7.0) with 3 mM HQ and 2 mM H_2O_2.

hybridization, the cluster-based nanoprobes were fabricated to further enhance the signal response.

According to the data from three independent electrochemical measurements, the detection precision was assessed with the relative standard deviations (RSD). When the concentration of cTnI was 50 ng/mL, the electrochemical aptasensor performed a RSD value of 4.3%. The result indicated that the established electrochemical method has excellent repeatability and precision.

3.6. Determination of cTnI in human serum sample

In order to investigate the practicality of the electrochemical aptasensor, the recoveries of different concentrations of cTnI in 100-fold-diluted human serum samples were measured by standard addition method. The prepared sample solution was incubated with the aptasensing interface to test the DPV signal. As shown in Table S2, the recovery of the aptasensor was in the range of 96.2%–102.0% and the

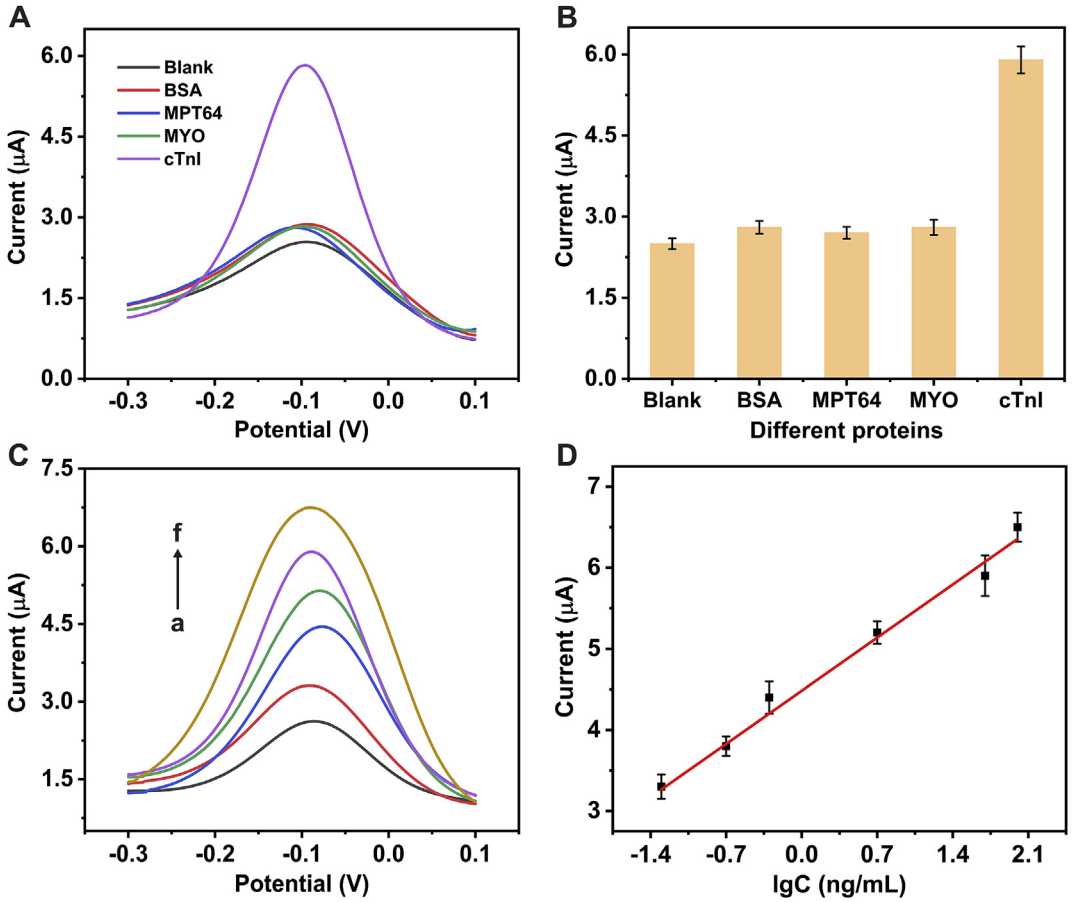

Fig. 4. (A) DPV responses and (B) the corresponding histogram obtained with various types of proteins with the same concentration (50 ng/mL). (C) DPV responses and (D) the logarithmic calibration curve of the aptasensor for the detection of cTnI with different concentrations (a–f: 0, 0.05 ng/mL, 0.5 ng/mL, 5 ng/mL, 50 ng/mL, and 100 ng/mL).

Table 1
Comparison of this electrochemical aptasensor with other reported aptasensors for cTnI detection.

Method	Immobilized receptor	Employed nanomaterial	Linear range (ng/mL)	Detection limit (pg/mL)	References
SWV	Tro4	Au@SiO_2@Au nanoparticles	0.024–240	30	Qiao et al. (2018)
SWV	Tro4	Si nanoparticles	0.024–240	24	Jo et al. (2015)
DPV	Aptamer	Au nanodumbbells	0.05–500	8	Negahdary et al. (2017)
DPV	Tro4	Au nanoparticles	0.024–2.4	24	Jo et al. (2017)
EIS	Tro4	MoS_2 nanosheets	0.024–24	23	Qiao et al. (2018)
Fluorescence	Tro4	Graphene oxide	0.10–6.0	70	Liu et al. (2018a)
ELISA	Antibody	Horseradish peroxidase	0.0312–1.0	10	This work
DPV	NTH-Tro4 + Tro6	Fe_3O_4@UiO-66/Cu@Au nanocomposites	0.05–100	16	This work

SWV: square wave voltammetry; DPV: differential pulse voltammetry; EIS: electrochemical impedance spectroscopy; ELISA: enzyme-linked immunosorbent assay.

RSD was in the range of 3.8%–5.9%. Furthermore, the practical application of the aptasensor was investigated by detecting cTnI in the blood serum samples of patients. The concentrations of cTnI in the diluted serum sample obtained with this aptasensor were consistent with those determined by the ELISA, as shown in Table S3. Hence, the aptasensor can effectively detect cTnI in human serum samples, proving that the developed method provides a potential clinic diagnostic tool for cTnI.

4. Conclusions

In summary, a novel nonenzymatic electrochemical aptasensor was designed for highly sensitive and selective detection of cTnI using NTH assisted dual-aptamer capture probes and cluster-based signal nanoprobes. With the assistance of DNA NTH structure, dual-aptamer technology, Fe_3O_4@UiO-66/Cu@Au hybrid nanozymes and LBL assembly method, supersandwich-type architectures were established on a SPGE interface. The enzyme-free aptasensor exhibits a low detection limit of 16 pg/mL, wide linear range, great repeatability and selectivity. In view of these advantages, this aptasensor will provide a potential application for cTnI detection in clinical research. Despite the significant developments in the electrochemical aptasensing of cTnI, there is no ideal device for clinic application. Future cTnI detection technology can be directed toward cost efficiency, multi-anlyte detection and shorter analytical time.

Declaration of interests

The authors declare that they have no known competing financial interests or personal relationships that could have appeared to influence the work reported in this paper.

CRediT authorship contribution statement

Duanping Sun: Conceptualization, Funding acquisition, Investigation, Methodology, Supervision, Validation, Writing - original draft. **Zibin Luo:** Data curation, Resources, Visualization. **Jing Lu:** Formal analysis, Funding acquisition, Resources, Software, Writing - original draft. **Shangshi Zhang:** Data curation, Formal analysis. **Tong Che:** Data curation, Formal analysis. **Zuanguang Chen:** Funding acquisition. **Luyong Zhang:** Funding acquisition, Project administration.

Acknowledgments

This work was supported by the National Natural Science Foundation of China (No. 81803521 and 21675177), the Natural Science Foundation of Guangdong Province (No. 2018A030310142), the Fundamental Research Funds for the Central Universities (No. 18zxxt69), the Medical Scientific Research Foundation of Guangdong Province (No. A2017033), and a Start-up Grant from Guangdong Pharmaceutical University (No. 51377003). The authors acknowledge the help from Dr. Xiangan Lin in Sun Yat-Sen Memorial Hospital for providing patient samples.

Appendix A. Supplementary data

Supplementary data to this article can be found online at https://doi.org/10.1016/j.bios.2019.03.049.

References

Abdorahim, M., Rabiee, M., Alhosseini, S.N., Tahriri, M., Yazdanpanah, S., Alavi, S.H., Tayebi, L., 2016. Trac. Trends Anal. Chem. 82, 337–347.
Akter, R., Jeong, B., Lee, Y.M., Choi, J.S., Rahman, M.A., 2017. Biosens. Bioelectron. 91, 637–643.
Chekin, F., Vasilescu, A., Jijie, R., Singh, S.K., Kurungot, S., Iancu, M., Badea, G., Boukherroub, R., Szunerits, S., 2018. Sens. Actuators B-Chem. 262, 180–187.
Dhawan, S., Sadanandan, S., Haridas, V., Voelcker, N.H., Prieto-Simon, B., 2018. Biosens. Bioelectron. 99, 486–492.
Fan, D.W., Bao, C.Z., Khan, M.S., Wang, C.L., Zhang, Y., Liu, Q.Z., Zhang, X., Wei, Q., 2018. Biosens. Bioelectron. 106, 14–20.
Goodman, R.P., Schaap, I.A.T., Tardin, C.F., Erben, C.M., Berry, R.M., Schmidt, C.F., Turberfield, A.J., 2005. Science 310, 1661–1665.
Han, X., Li, S.H., Peng, Z.L., Othman, A.M., Leblanc, R., 2016. ACS Sens. 1, 106–114.
Jo, H., Gu, H., Jeon, W., Youn, H., Her, J., Kim, S.K., Lee, J., Shin, J.H., Ban, C., 2015. Anal. Chem. 87, 9869–9875.
Jo, H., Her, J., Lee, H., Shim, Y.B., Ban, C., 2017. Talanta 165, 442–448.
Kemp, M., Donovan, J., Higham, H., Hooper, J., 2004. Br. J. Anaesth. 93, 63–73.
Lin, M.H., Song, P., Zhou, G.B., Zuo, X.L., Aldalbahi, A., Lou, X.D., Shi, J.Y., Fan, C.H., 2016. Nat. Protoc. 11, 1244–1263.
Liu, D.K., Lu, X., Yang, Y.W., Zhai, Y.Y., Zhang, J., Li, L., 2018a. Anal. Bioanal. Chem. 410, 4285–4291.
Liu, P., Han, L., Wang, F., Li, X.Q., Petrenko, V.A., Liu, A.H., 2018b. Nanoscale 10, 2825–2833.
Ma, X.W., Wen, S.S., Xue, X.X., Guo, Y., Jin, J., Song, W., Zhao, B., 2018. ACS Appl. Mater. Interfaces 10, 25726–25736.
Nandhikonda, P., Heagy, M.D., 2011. J. Am. Chem. Soc. 133, 14972–14974.
Negahdary, M., Behjati-Ardakani, M., Sattarahmady, N., Yadegari, H., Heli, H., 2017. Sens. Actuators B-Chem. 252, 62–71.
Nezami, A., Dehghani, S., Nosrati, R., Eskandari, N., Taghdisi, S.M., Karimi, G., 2018. J. Pharmaceut. Biomed. 159, 425–436.
Qiao, X.J., Li, K.X., Xu, J.Q., Cheng, N., Sheng, Q.L., Cao, W., Yue, T.L., Zheng, J.B., 2018. Biosens. Bioelectron. 113, 142–147.
Rezaei, B., Ghani, M., Shoushtari, A.M., Rabiee, M., 2016. Biosens. Bioelectron. 78, 513–523.
Smith, J.G., Gerszten, R.E., 2017. Circulation 135, 1651–1664.
Song, Y.P., Duan, F.H., Zhang, S., Tian, J.Y., Zhang, Z.H., Wang, Z.W., Liu, C.S., Xu, W.M., Du, M., 2017. J. Mater. Chem. 5, 19378–19389.
Sun, D.P., Lu, J., Chen, D.B., Jiang, Y.F., Wang, Z.R., Qin, W.W., Yu, Y.Y., Chen, Z.G., Zhang, Y.Q., 2018a. Sens. Actuators B-Chem. 268, 359–367.
Sun, D.P., Lu, J., Luo, Z.F., Zhang, L.Y., Liu, P.Q., Chen, Z.G., 2018b. Biosens. Bioelectron. 120, 8–14.
Sun, D.P., Lu, J., Zhong, Y.W., Yu, Y.Y., Wang, Y., Zhang, B.B., Chen, Z.G., 2016. Biosens. Bioelectron. 75, 301–307.
Takeda, S., Yamashita, A., Maeda, K., Maeda, Y., 2003. Nature 424 (6944), 35–41.
Tan, Y., Wang, Y.Y., Li, M.S., Ye, X.X., Wu, T.H., Li, C.Y., 2017. Biosens. Bioelectron. 91, 741–746.
Wang, Q.Q., Wei, H., Zhang, Z.Q., Wang, E.K., Dong, S.J., 2018. Trac. Trends Anal. Chem. 105, 218–224.
Wei, H., Wang, E.K., 2013. Chem. Soc. Rev. 42, 6060–6093.
Yan, H.X., Tang, X.D., Zhu, X.D., Zeng, Y.B., Lu, X., Yin, Z.Z., Lu, Y.X., Yang, Y.W., Li, L., 2018. Sens. Actuators B-Chem. 277, 234–240.
Yang, F., Li, Q., Wang, L.H., Zhang, G.J., Fan, C.H., 2018a. ACS Sens. 3, 903–919.
Yang, X., Yu, Y.Q., Peng, L.Z., Lei, Y.M., Chai, Y.Q., Yuan, R., Zhuo, Y., 2018b. Anal. Chem. 90, 3995–4002.
Ye, X.S., Shi, H., He, X.X., Wang, K.M., He, D.G., Yan, L.A., Xu, F.Z., Lei, Y.L., Tang, J.L., Yu, Y.R., 2015. Anal. Chem. 87, 7141–7147.
Zhang, L., Xiong, C.Y., Wang, H.J., Yuan, R., Chai, Y.Q., 2017. Sens. Actuators B-Chem.

241, 765–772.
Zhang, T., Ma, N., Ali, A., Wei, Q., Wu, D., Ren, X., 2018a. Biosens. Bioelectron. 119, 176–181.
Zhang, Y., Wang, F.M., Liu, C.Q., Wang, Z.Z., Kang, L.H., Huang, Y.Y., Dong, K., Ren, J.S., Qu, X.G., 2018b. ACS Nano 12, 651–661.
Zhao, H.X., Zou, Q., Sun, S.K., Yu, C.S., Zhang, X.J., Li, R.J., Fu, Y.Y., 2016. Chem. Sci. 7, 5294–5301.
Zheng, T.T., Zhang, Q.F., Feng, S., Zhu, J.J., Wang, Q., Wang, H., 2014. J. Am. Chem. Soc. 136, 2288–2291.